Fabrication of Functionalised Nanobiomaterial for Removal of Hg(II) Ions: Thermodynamic and Kinetic Adsorption Studies

Genji Jaishree, Gorli Divya and Tirukkovalluri Siva Rao[*]

Department of Inorganic and Analytical Chemistry, Andhra University,
Visakhapatnam 530003, India
[*]Corresponding author (e-mail: sivaraoau@gmail.com)

This article is focused on the fabrication of functionalized activated carbon material to improve its adsorption performance in the removal of Hg(II) ions. To increase its surface area, the above material was subjected to the ball milling process to obtain Ball Milled Activated Carbon (BMAC). The BMAC was characterized by Fourier Transform Infrared Spectroscopy (FTIR), Scanning Electron Microscopy (SEM), and Branauer-Emmet-Teller (BET) analysis. The characterisation results are evidence of the successful impregnation of functional groups such as PO_4^{3-} and SO_4^{2-} ions as well as irregular cave-type openings in BMAC with large pore sizes and high surface areas (524 m^2/g). To further improve the efficiency of BMAC in the adsorption of Hg(II) ions, various parameters were studied and optimized to the following: 120 min contact time, pH 4, adsorbent dosage 4.0 g, 20 mg/L Hg(II) ion concentration, and 60 °C temperature. The experimental data fit well with the Freundlich adsorption isotherm and followed First Order kinetics. The positive ΔH and the negative ΔG values confirm that the adsorption reaction was endothermic and spontaneous.

Toxic heavy metals are one of the contributing factors to environmental pollution due to their entry into the environment through natural calamities such as volcanic eruptions, earthquakes, or storms. The enrichment of these metal ions in the environment occurs via different anthropogenic industries like mining, agrochemical plants, and metallurgical industries. Their degree of toxicity in the environment increases due to their persistence, nonbiodegradability, and ability to enter the food chain [1,2]. Mercury is a toxic element that has been found in the environment both naturally and as an introduced contaminant which can be further converted into organic mercurials (methyl mercury) which have very high levels of toxicity [3]. The increasing levels of these pollutants may be due to the lack of suitable environment-friendly treatment techniques. Consequently, there is a critical need to remove mercury(II) ions from polluted wastewater. For many years, conventional methods have been used for the removal of these toxic metals such as coagulation, flocculation, membrane filtration, and precipitation [4]. These methods are efficient at an appropriate concentration of toxic metals but they lose their efficiency at low concentrations [5]. More recently, physicochemical, electrochemical, and solvent extraction methods were developed to remove toxic metals even at low concentrations, but these suffer from serious drawbacks including cost, high energy consumption, and by-products that are nonbiodegradable secondary

pollutants [6,7]. Hence it has become a prime concern for many researchers to develop a green approach. For the last few years, bioadsorption has been promising, due to its cost-effectiveness, eco-friendliness, and non-polluting features [8]. Activated carbon, a widely used adsorbent material in industry, is of limited use as it raises the cost of the process [9]. Important features of high-quality activated carbon include a high carbon content, a low ash content, a low sulphur content, as well as a low content of other impurities, such as chloride and heavy metals.

In the recent past, several bioadsorption studies have been conducted using biomaterials obtained from agricultural wastes like sugarcane bagasse [10], soya bean hulls [11], walnut hulls [12], cottonseed hulls [13], corn cobs [14], etc. Agriculturally-derived activated carbon (AC) has a high ash content. Apart from these, the ACs derived from plant parts such as roots, stems, bark, flowers, leave, and fruit peels, have an added advantage over agricultural waste derived ACs as they are mainly composed of cellulose, hemicelluloses, lignin, lipids, protein, sugar, water, hydrocarbon, starch with many functional groups capable of removing toxic compounds from waste-water sources with high carbon content and low ash content [15].

Functionalization of activated carbon further promotes adsorption kinetics by the introduction of

charged groups. In view of this, several researchers have worked on the functionalization of activated carbon treated with KOH, $ZnCl_2$, NaOH, $CaCl_2$, H_2SO_4, and H_3PO_4. Amongst them, only H_2SO_4- and H_3PO_4-treated activated carbon were shown to have high adsorption affinities owing to an increase in surface area. Budinova et al. [16] reported that among all acids, H_3PO_4-impregnated activated carbon showed a high surface area followed by steam vaporization at high temperatures. Moulefera et al. [17] also reported that phosphoric acid impregnated porous activated carbon had an enhanced surface area, but with the requirement of high-temperature thermal treatment. Prakash et al. [18] and his co-workers reported that H_2SO_4-impregnated activated carbon pyrolysed at different temperatures between 723 to 1223 K. Kolur et al. [19] mentioned that a high H_2SO_4 content blocks the pores and produces high ash content, while Ademiluyi et al. also reported high ash content at high temperatures [20]. In addition, the impregnation ratio plays a vital role in determining the surface properties of activated carbon [21]. Hence based on the above flaw rather than the preparation of monofunctionalized activated carbon, it is appropriate to introduce bifunctional (PO_4^{3-} and HSO_3^-) groups to achieve high adsorption capacity in the removal of metal ions. Hg(II) has been widely reported to damage the lungs, respiratory tract, bronchus, and kidney, and even cause death [22].

Hence the present research work has mainly focused on the fabrication of bifunctionalized activated carbon from *Calotropis procera* stems, and studied its effectiveness in adsorbing toxic Hg(II) ions, by evaluating the adsorption equilibrium using best-fit adsorption isotherm models.

The present study aims to evaluate the potential of acid-treated activated carbon produced from abundantly available *Calotropis procera* stems. The novelty of the present study is two-fold: (1) introduction of bifunctional groups into activated carbon by controlled carbonization with reduced ash content, and (2) promotion of adsorption of the adsorbate on the adsorbent by increasing its surface area through conversion into nano biomaterials by ball-milling. *Calotropis procera*, a locally and abundantly available shrub can be exploited as a major source of carbon due to its high carbon content (78.03%) [23] and carboxylic ester side chains that promote attachment of positive metal ions [24]. Further, the best-fit adsorption isotherm models will be studied in order to establish an equilibrium relation between the concentration of adsorbate in solution and the adsorbent dose. The disposal of spent adsorbent and the recovery of adsorbed Hg(II) ions are also matters of concern, paving the way for the employment of various non-destructive regeneration techniques [25], of which chemical regeneration using HCl is most efficient due to less deterioration, low ash content and high recovery efficiency observed for the removal of Hg(II) ions [26]. Patel et al. reported that the column desorption method was found to be efficient for acidic eluents, with high eluent efficiency and low adsorbent loss observed for 5 consecutive cycles [27]. Thus the desorption studies herein were carried out utilizing the column method with an optimum concentration of HCl as the eluent.

EXPERIMENTAL

Biomaterials, Chemicals and Solution Preparation

Calotropis procera stems were used as a precursor for the preparation of activated carbon. H_2SO_4 50 wt % and H_3PO_4 50 wt % (Merck, Darmstadt, Germany) were used in different ratios (H_2SO_4: H_3PO_4 of 1:9, 2:8, and 3:7) for carbonization and impregnation of the PO_4^{3-} and SO_4^{3-} groups. Freshly prepared 0.1M HCl or NaOH solutions were used to adjust the pH during the adsorption studies. The stock solution of $HgCl_2$ (1000 mg/L in deionized water) was used as a source precursor for Hg(II) in slightly acidic conditions. The Hg(II) ion concentration was varied in the range of 5-100 mg/L and obtained by dilution of the stock solution for batch adsorption studies.

Instrumental Techniques Employed for the Preparation of Bionanomaterial, Characterisation and Adsorption Studies

Ball milling is a green mechanochemical approach, generally employed in low-temperature alloy processing. This High Energy Ball Mill (EMAX, Retsch, INDIA) technique is utilized to convert the biomaterial into bionanomaterial, which is a prime requisite for efficient adsorption of toxic metals due to the increase in surface area. Fourier-transform infrared (FTIR) spectra of the sample were recorded from 4000–400 cm^{-1} with a JASCO 4100 FTIR spectrometer (Jasco International, Tokyo, Japan) in transmission mode using the KBr pellet method, for detection of functional groups introduced during the process. The morphology of BMAC was analysed using a scanning electron microscope (ZEISS SIGMA FE-SEM) equipped with an energy dispersive X-ray spectrophotometer (EDX) with a resolution of 1 nm @ at 15 kV with HD. The pore volume (V_P), pore size, and surface area analysis (S_{BET}) of BMAC were determined by the N_2 adsorption-desorption isotherm curve at 77.3 K using a Brunauer-Emmett-Teller (BET) surface area analyzer (Quanta chrome Nova 2200 E System). An orbital shaker (EIS 35S LABZEE BIOTECH, INDIA) was used for the agitation process during the adsorption of Hg(II) ions on functionalized activated carbon. A Varian SpectrAA 800 Atomic Absorption Spectrometer equipped with a GTA 100 graphite furnace Zeeman background correction and a mercury hollow cathode lamp (Varian) was used to determine the concentration of Hg(II) by adsorption studies.

Conversion of Biomass into Activated Carbon

The fresh *Calotropis procera* stems were collected from the local shrubs available on the campus premises of Andhra University in Vishakapatnam, India. The biomass was cut into pieces and then washed with deionized water to remove dirt or other particulate matter, shade dried for 2-3 days and then finely ground. The obtained ground biomass was soaked overnight in 50 wt % mixtures of H_2SO_4 and H_3PO_4 in different ratios (1:9, 2:8, and 3:7) in laboratory conditions at room temperature. The activated carbon (AC) thus obtained was washed with deionized water to remove unreacted acid and then dried in an oven at 80 °C for 12 h. The different ratios of functionalized activated carbon samples, were labelled AC1, AC2, and AC3 corresponding to 1:9, 2:8, and 3:7, respectively, and stored in airtight containers in a desiccator to avoid moisture.

The three types of ACs were analysed for their quality by conducting proximate analyses using ISI standard procedures [3rd Revision, 2004] and the results are compared in Table 1. AC1 (1:9) was found to be the best in terms of its characteristics such as complete carbonization, low ash content, high ion exchange capacity, low apparent density, and high total carbon content desirable for high grade activated carbon. There was a direct relationship between the increase in ash content and the decrease in adsorption capacity. The fixed carbon content of a given dry BMAC1 is normally obtained by subtracting the ash content (which represents the inorganic portion of the carbon) from 100, which was 71.5 % in this case. The ash content was limited to 28.5 %, accounting for one-third of the total carbon content, to achieve the best adsorption performance and high surface area. The as-obtained AC1 was further pulverised to nano size using high-energy ball milling and this was labeled BMAC (Ball Milled Activated Carbon). The surface area before and after ball milling was obtained from the BET (surface area analyzer) and discussed in the BET analysis section.

Table 1. Proximate Analysis of the chemical and textural properties of synthesized AC1, AC2 and AC3.

Parameter Analysed	Results		
	AC1	AC2	AC3
Moisture content (%)	8.80	10.20	15.60
Ash content (%)	28.50	42.30	56.53
Total carbon (%)	71.5	57.70	43.47
Apparent density (g/mL)	0.35	0.43	0.62
Matter soluble in water (%)	0.18	0.22	0.28
Matter soluble in acid (%)	0.12	0.25	0.38
pH of the carbon (water extract)	3.23	2.28	1.76
Ion exchange capacity (meqts/ gm)	1.02	0.92	0.79
Methylene blue value (mg/g)	18.0	14.0	10.0
Phenol number (mg/g)	88.0	65.0	58.4
Iron (%)	0.054	0.068	0.083
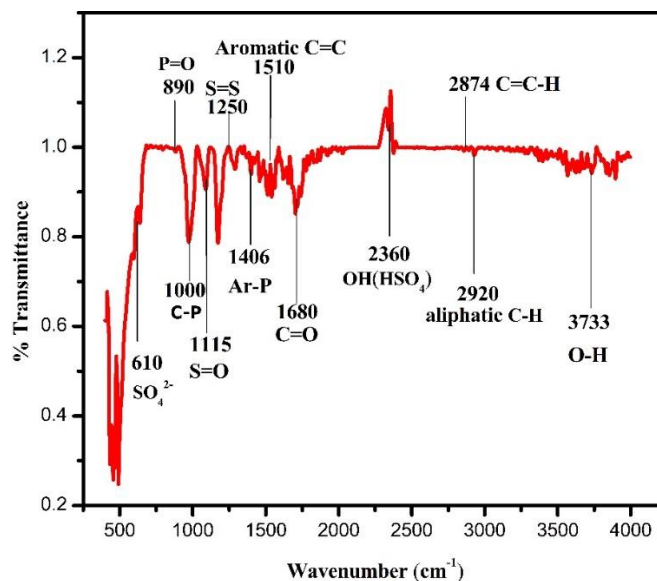
Figure 1. FTIR analysis of BMAC.

Table 2. Some fundamental measured IR absorption frequencies of sulfurized and phosphorylated BMAC.

No.	Band position (cm^{-1})	Possible assignments
1	610	Bisulphate ion (SO$_4{}^{2-}$)
2	890	P-O
3	1100	(P-O) Phosphate ester
4	1115	S=O Stretching
5	1180	Hydrogen bonded P=O
6	1250	C-S Stretching.
7	1406	Aromatic C-P
8	1510	Aromatic C=C
9	2920	Aliphatic C-H
10	2874	C=C-H Stretching, doublet, sharp and small
11	3733	OH Stretching, weak, and very broad-bonded

Characterization of BMAC using Different Instrumental Techniques

FTIR Analysis

The impregnated phosphate and sulphate acid groups were identified using the FTIR spectrum as recorded in Figure 1.

Figure 1 depicts the FTIR spectra of BMAC. The peak values at different band positions correspond to different functional groups which account for the structural and chemical characteristics of BMAC. The intense peak observed at 3733 cm^{-1} is attributed to the surface hydroxyl groups of carboxylic acids, alcohols, or H$_2$O adsorbed on the surface [26], while the bands at 2920 cm^{-1} [28], and 2874 cm^{-1} [29] correspond to the methyl and methylene C-H bonds, respectively. The bands at 1115 cm^{-1} [30] and 1250 cm^{-1} [31] are attributed to the S=O and C-S stretching which indicates the presence of sulfate and which is further confirmed by the presence of a peak at 610 cm^{-1} corresponding to the bisulfate ion [19]. Further, the presence of bands at 890, 1100, 1180, and 1406 cm^{-1} correspond to free (P=O) [32], (P-O) derived from phosphate ester [26], hydrogen-bonded (P=O) [33] and phosphorous bonded to aromatic rings [34], respectively. The presence of these peaks confirms the

successful impregnation of BMAC with HSO_4^- and PO_4^{3-} in the ratio of 1:9. The additional peak at 1510 cm^{-1} derived from the aromatic C=C group shows the presence of aromatic rings in the obtained BMAC [35]. The functionalisation of activated carbon promotes adsorption due to the presence of phosphate. During the activation, depolymerization, dehydration, and redistribution of constituent biopolymers causes the conversion of aliphatic to aromatic rings [34]. The corresponding stretching frequencies of the functional groups in activated carbon are given in Table 2.

BET Surface Area Analysis

The N_2 adsorption desorption isotherms and BJH pore size distribution curves for BMAC prepared by

impregnation of H_2SO_4 and H_3PO_4 in the ratio 1:9 are shown in Figure 2(a) and (b), indicating a H_2 hysteresis loop with type IV isotherm characteristics of the ordered macroporous structure. Before ball milling, the BET surface area was found to be 243 m^2/g with pore volume of 0.204 cm^3/g and pore size of 4.8 nm. After ball milling, the BET surface area was 524 m^2/g, pore volume 0.318 cm^3/g and pore size 60.56 nm, and these increased values confirmed the pulverisation of biomaterial using the ball mill. Treatment of activated carbon with H_2SO_4 at low temperatures promotes the decomposition of polymeric structures and gasification of non-carbon elements yielding a highly porous carbon which in turn facilitates the adsorption of toxic metals [36].
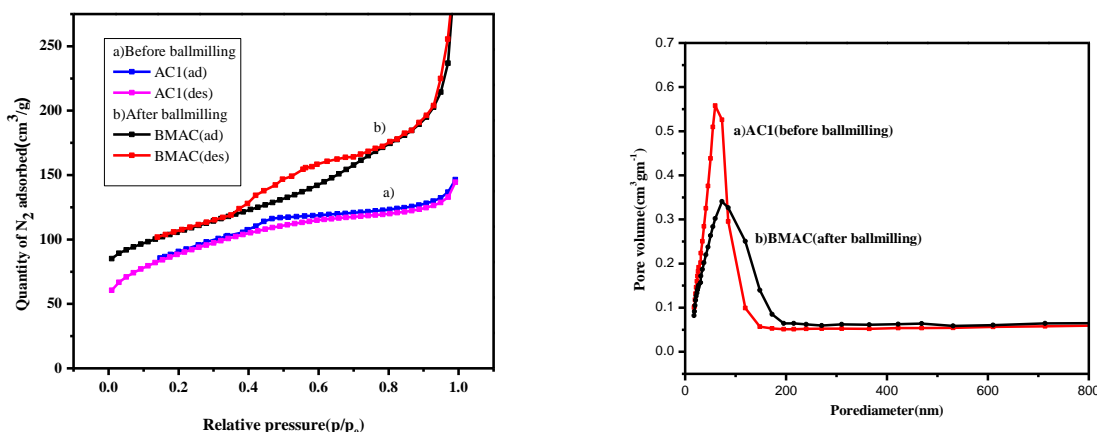
Figure 2. a) N_2 adsorption–desorption isotherms and b) BJH pore size distribution curves for BMAC.

Elements	Weight%	Atomic%
C	61.68	60.22
O	33.64	34.17
P	4.625	3.752
S	0.425	0.416
Total	100	100
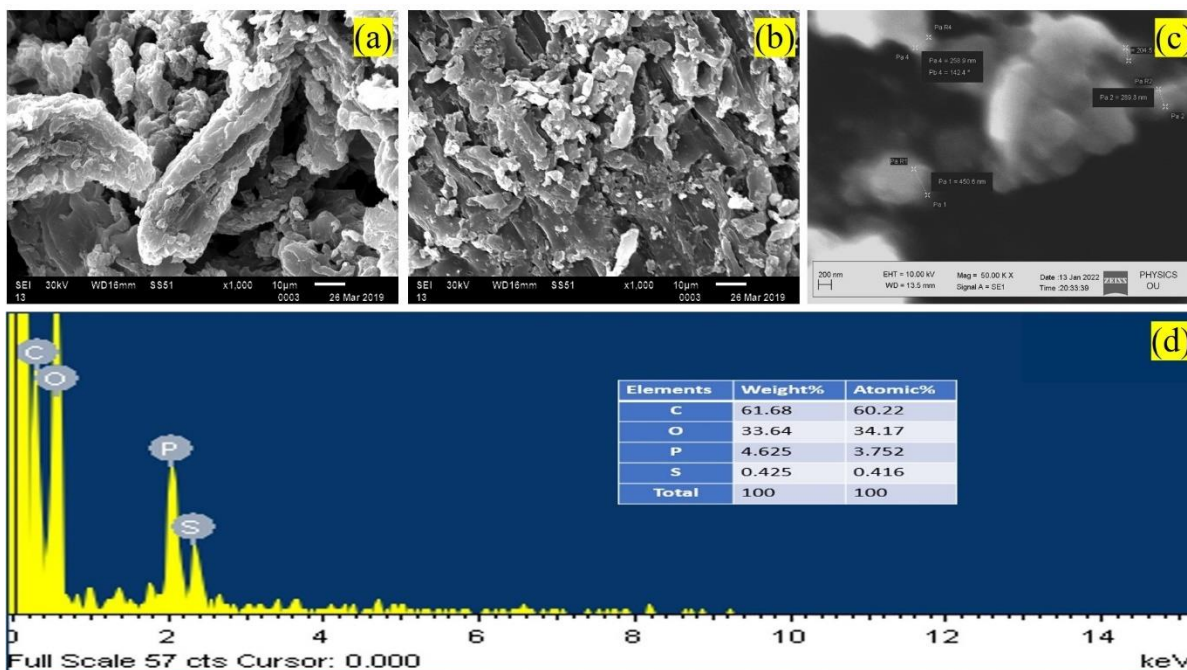
Figure 3. SEM images of BMAC a) before ball milling, b) after ball milling, c) high resolution image after ball milling, and d) EDX analysis.

SEM EDX Analysis

The morphology of activated carbon before and after ball milling can be seen in Figure 3(a) and (b) respectively. It clearly shows the irregular surface, presence of bigger holes, and cave-type openings on the surface. This indicates that the highly porous nature of BMAC is more favourable for the trapping of toxic metal ions by the impregnated functional groups in the pores and caves. The EDX analysis (Fig. 3c) shows the presence of carbon (C), phosphorous (P), oxygen (O), and sulfur (S) attributed to the presence of impregnated groups in BMAC.

Adsorption of Hg(II) Ions on BMAC

Experiments were performed by the addition of desired concentrations of Hg(II) ion solutions (5-100mg/L) and adsorbent (0.5-5.0 g) to 150 mL conical flasks maintained at a pH ranging from 2 to 7 and agitated using the EIS 35S orbital shaker with a rotating speed of 350 rpm for 3 h until equilibrium was achieved. The aliquots were taken at different time intervals and analysed for the decrease in metal ion concentration with time using AAS. The percent removal of metal ions can be calculated using Equation (1).

$$\% \, Adsorption = (C_i - C_f)/C_i \times 100 \qquad (1)$$

Where C_i = initial concentration of the metal ion, C_f = final concentration of the metal ion in the solution.

Different parameters were studied and optimized to obtain the best adsorbent dosage, pH, metal ion concentration, contact time and temperature, by continuously varying one parameter while keeping others constant.

Desorption and Regeneration Studies of Hg(II) Ions on BMAC

The desorption process was carried out using the column method. Here, the spent BMAC (containing adsorbed Hg(II) ions) was filtered off and washed using deionized water to remove the unadsorbed Hg(II) ions. The BMAC was then packed into a column and 0.1 M HCl was passed through the column at a slow rate while the pH was adjusted in the range of 2-6 in the subsequent desorption process. Then the column was rinsed with 50 mL deionized water and the concentration of Hg(II) ions was determined using AAS. The % desorption was calculated using Equation (2).

$$\% \, Desorption = C_{des}/C_{ads} \times 100 \qquad (2)$$

where C_{des} and C_{ads} (mg/L) represent the concentration of Hg(II) ions in desorbed and adsorbed phases, respectively.

The reusability of BMAC for the adsorption of Hg(II) was studied for subsequent cycles. For this purpose, the regenerated packed BMAC column was removed, washed several times with deionized water and dried in an oven at 80 °C for 12 h and was studied for 5 consecutive cycles.
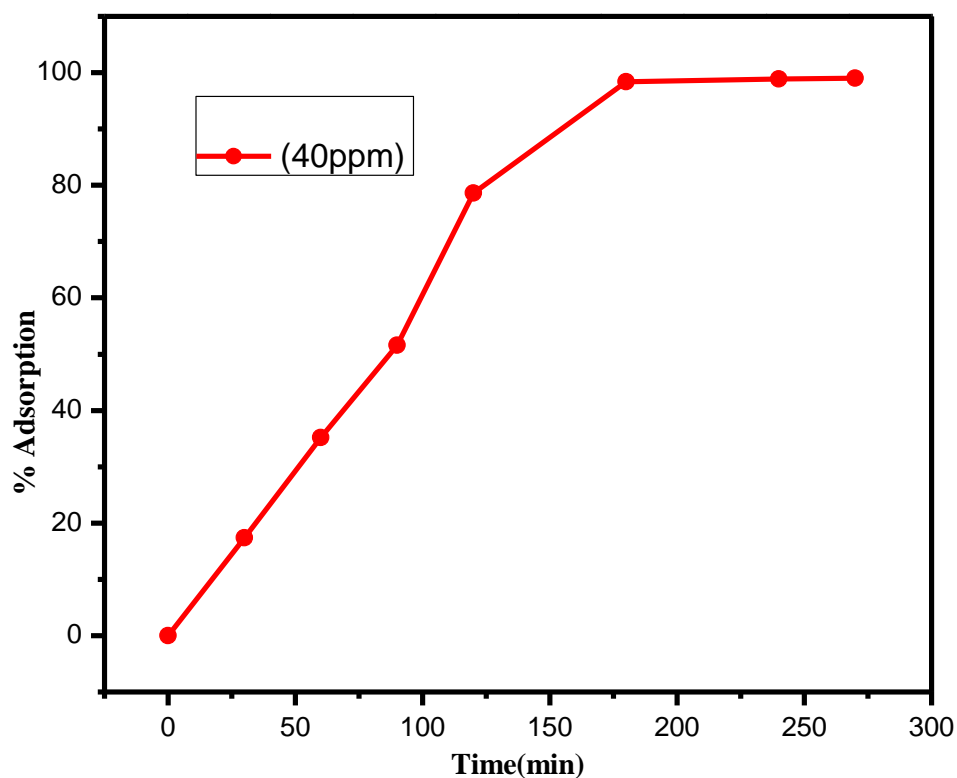
Figure 4. Effect of contact time on adsorption of metal ions (40 mg/L Hg(II)).

RESULTS AND DISCUSSION

Optimisation of Parameters for Better Adsorption of Hg(II) on BMAC

Influence of Contact Time

The influence of contact time on the adsorption of BMAC was studied in the range of 0 to 300 min at 25 min intervals. The experiments were carried out using 40 mg/L Hg(II) solution and 2.5 g of carbon maintained at pH 4 at 25 °C and agitated at 250 rpm.

The results presented in Figure 4 reveal a rapid increase in % adsorption of Hg(II) ions which then diminished gradually to attain equilibrium within 180 min. This may have resulted from the fact that there is a direct relationship between the metal ion concentration and time; the lower the concentration, the lesser the time needed to attain equilibrium. However, the stabilization of adsorption due to saturation requires time. Taking into consideration the above facts, the contact time was fixed at 180 min for subsequent studies and other parameters were varied to determine optimum conditions.
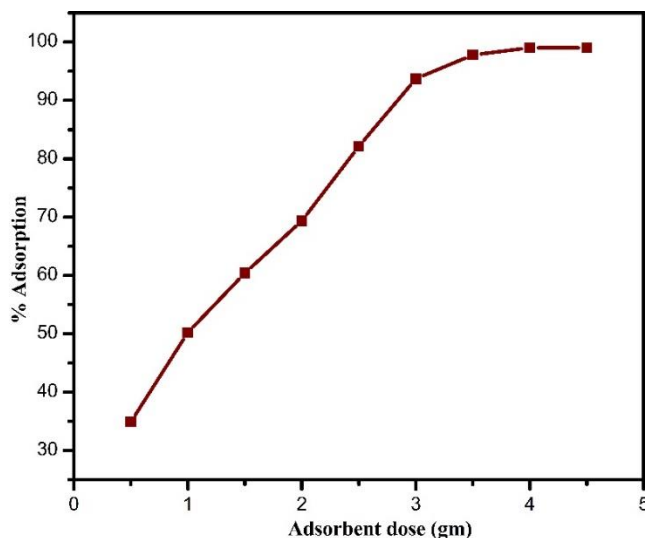
Figure 5. Effect of adsorbent dose in 180 min.
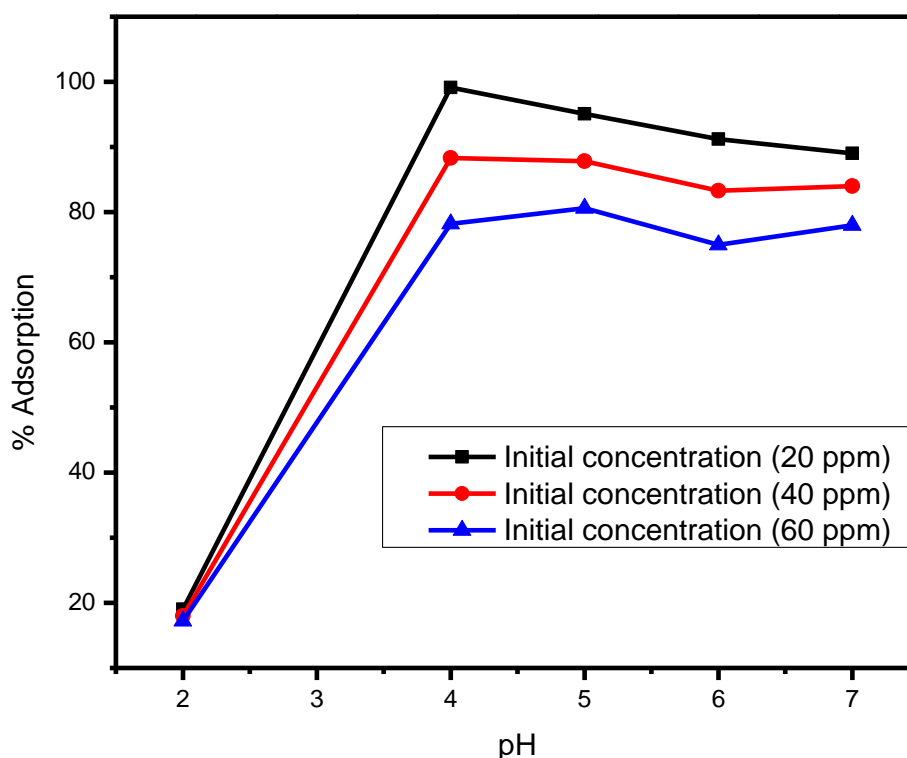
Figure 6. Effect of pH on BMAC (adsorbent dosage 4.0 g, duration 150 min).

Significance of Adsorbent Dose

A study on the effect of the adsorbent dose on the adsorption of Hg(II) ions was carried out by varying the dose from 0.5 g to 5.0 g at increments of 0.5 g with other parameters kept constant (pH 4, 40 mg/L initial Hg(II) concentration, 25 °C). The results are shown in Figure 5. It can be inferred from the figure that the adsorption efficiency increases up to an adsorbent dosage of 4.0 g, beyond which the peak levelled off due to the attainment of adsorption-desorption equilibrium within 150 min. At the initial stage, the rise in the adsorption percentage was due to the large number of available adsorbent particles for the adsorption process. At a high dosage of adsorbent, the non-availability of sufficient metal ions led to a reduction in adsorption % per unit mass of adsorbent.

Role of pH on BMAC Adsorption

The solution pH greatly affects the surface charge properties of the adsorbent, which in turn influences the adsorption of metal ions on the active sites of the adsorbent. The effect of pH on the adsorption of Hg(II) ion to BMAC was studied by varying the pH from 2 to 7 with other parameters kept constant (150 min contact time, 4 g adsorbent, 40 mg/L initial Hg(II) concentration, 25 °C). The experimental results are presented in Figure 6. It can be inferred from this figure that there was a gradual increase in metal ion adsorption up to pH 4 within 140 min, after which the value became constant. This may be due to the

competition between H^+ and Hg^{2+} for the negative active sites on the adsorbent in low pH conditions [25]. Further, at pH 4 there is a decrease in H+ ion concentration where the charges of the metal ions and the negative active sites equilibrate and the curve becomes constant even though the pH is increased. The removal of Hg(II) ions can be best explained based on the surface complexation theory [37]. The following surface complexes are formed when Hg (II) is present in the solution with the functional groups present on the carbon:

$$2(C_xSO_3H) + Hg^{2+} \longrightarrow (C_x SO_3)_2 Hg^{2+} + 2H^+$$

$$2(C_xPO_4H_2) + 2Hg^{2+} \longrightarrow (C_xPO_4)_2 Hg_2^{2+} + 2H^+$$
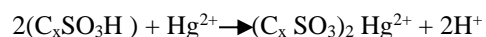
Impact of Initial Metal Ion Concentration

In this study certain parameters were maintained constant (adsorbent dosage 4.0 g, contact time 140 min, and pH 4 at 25 °C) while the initial Hg(II) ion concentration was varied. Figure 7 shows the interdependency of adsorption (%) with the initial concentration of Hg(II) ions. The initial metal ion concentration was increased from 5 mg/L to 100 mg/L in increments of 20 mg. The adsorption appeared to increase from 5 to 20 mg/L within 130 min, beyond which it decreased. At low metal ion concentrations, more active sites are available; as the concentration of metal ions increases, charge saturation is reached at 20 mg/L.
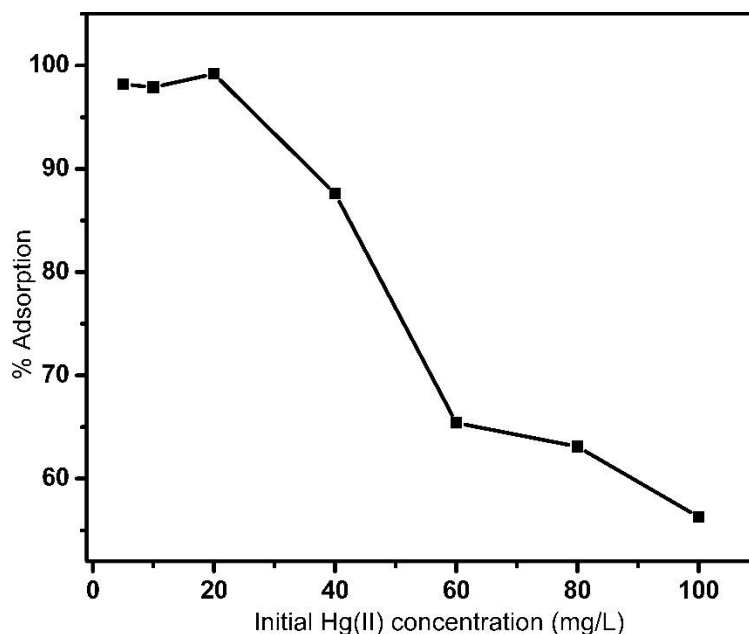
Figure 7. Effect of initial concentration of Hg(II) (Adsorbent dosage 4.0 g, contact time 140 min and pH 4).
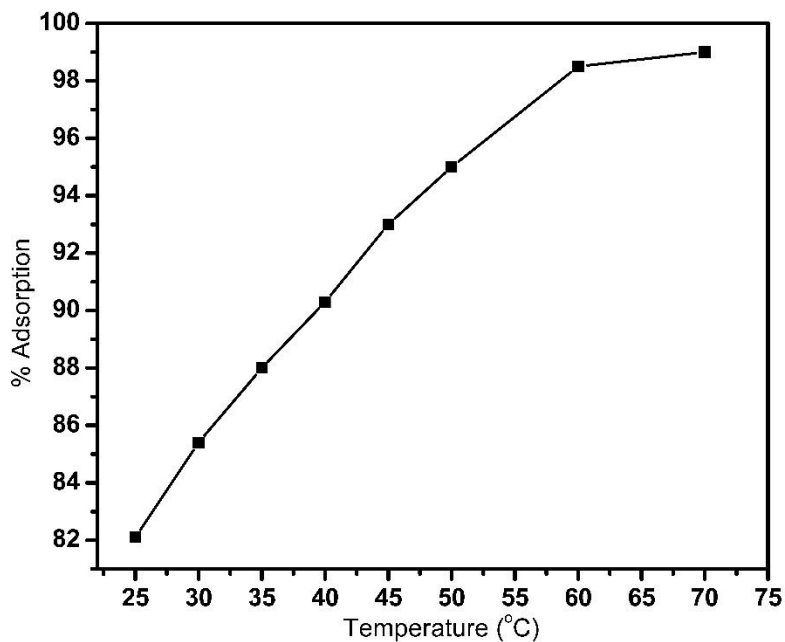
Figure 8. Effect of temperature on adsorption (adsorbent dosage 4.0 g, duration 130 min, pH 4)

Consequences of Varying Temperature with 20 mg/L of Adsorbate

The influence of temperature on adsorption was studied from 25-70 °C at increments of 5 °C. The results are depicted in Figure 8, which indicates that there is a direct relationship between adsorption efficiency and temperature. This can be attributed to the fact that with increasing temperature, the mobility and solubility of Hg(II) ions increases and thus the extent of adsorption increases [38], and within 120 min contact time up to 99% adsorption was achieved. In addition, an increase in temperature facilitates the broadening and deepening of pores, which in turn enhances adsorption through a phenomenon known as activated diffusion [39]. The promoted diffusion of metal ions is evident in the endothermic nature of the reaction.

Hence at 120 min, with an adsorbent dose of 4 g, Hg(II) ion concentration of 20 mg/L, and a pH 4 solution maintained at 60 °C, the rate of adsorption of Hg(II) ions on BMAC was found to be 99%. After achieving the optimized parameters, desorption studies were carried out using the column method, keeping all parameters at optimum levels except for pH, which was varied from 2 to 6. The adsorbent BMAC after desorption of the ions
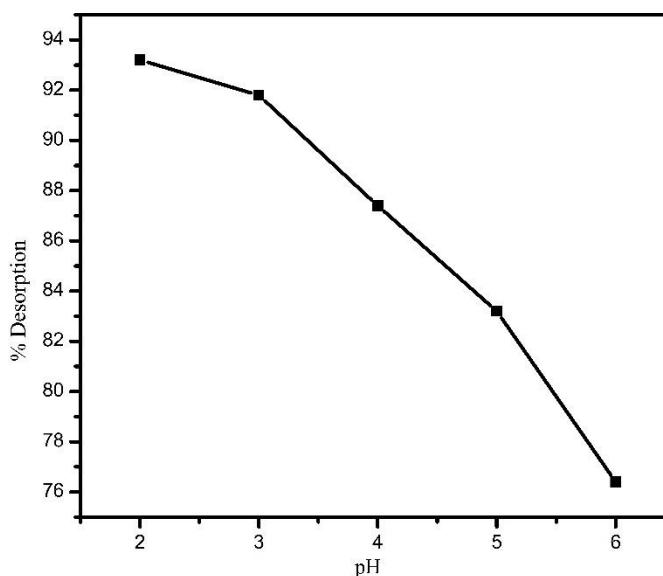
Figure 9. Desorption of Hg(II) ions with increasing pH.

was checked for further adsorption capacity. The reuse of regenerated activated carbon was found to be efficient up to 5 cycles, beyond which the adsorption remained almost constant. In the 2nd cycle, the adsorption efficiency was found to increase due to the elution of some impurities leading to enhanced exposure of pores towards Hg(II) ions [40]. The results are presented in Figures 9 and 10. The results of this study were compared with those from previous work using different adsorbents, as listed in Table 3 [41, 42, 43].

It can be inferred from Figure 9 that at pH 2, due to abundant availability of H^+ ions, rapid exchange of Hg(II) with H^+ ions takes place which in turn facilitates easy desorption (93%) of Hg(II). With an increase in pH, fewer H^+ ions are available, thus the exchange of H^+ ions with Hg(II) is slower and the % desorption decreases. At pH 2, the predominant species is $HgCl_4^{2-}$ but when the pH

increases the dominant species is $HgCl_3^-$, so at low pH there is more repulsion between negatively charged surface groups (HSO_4^- and PO_4^{3-}) and $HgCl_4^{2-}$ which favours the desorption process [43].

Study of Thermodynamic Parameters

The values for ΔH and ΔS were calculated from the slope and intercept of the linear Van't Hoff plot, respectively, using the relation:

$$\ln K_d = \frac{\Delta S}{R} - \frac{\Delta H}{RT} \tag{3}$$

Where: ΔS = entropy change for the process
ΔH = enthalpy change for the process
R = gas constant
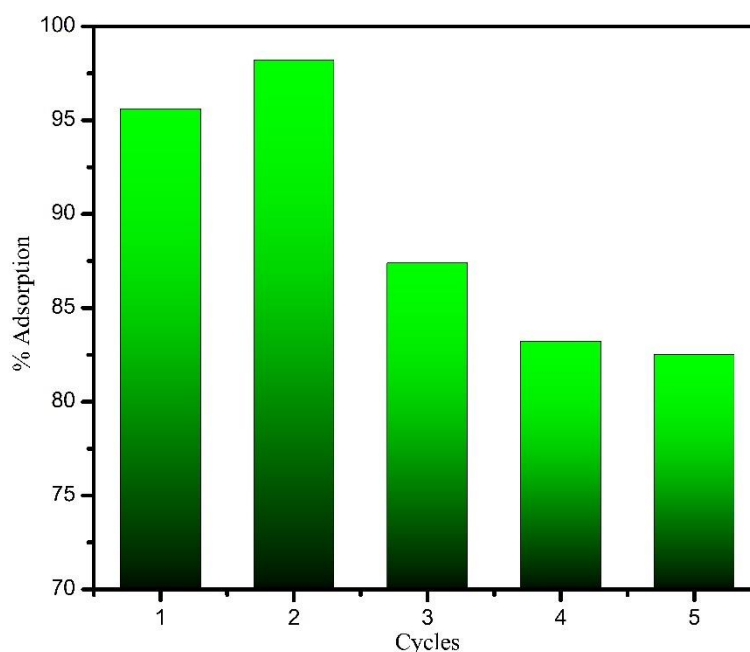
Figure 10. Recyclability of BMAC towards Hg(II) ion removal.

Table 3. Comparative reports on the adsorption of Hg(II) ions by various adsorbents.

Serial number	Biomaterials	Activating agent	%Adsorption	Contact time (min)	Ref No.
1	Date pits	Sulfur/Silane	93.7	300	41
2	Aracea Nut Shell	Succinic Anhudride	68.0	300	42
3	Coconut Shell	Copper Chloride	85.7	90	43
4	*Calotropis procera* stem	H_2SO_4: H_3PO_4 1:9	99	120	Present work

The distribution coefficient (K_d) of the activated charcoal surface was calculated using Equation (4) given below.

$$K_d = \frac{C_i - C_e}{C_e} \times \frac{V}{m} \left(mLg^{-1} \right)$$

(4)

The changes in free energy (ΔG) for the specific adsorption were also calculated using the equation (5):

$$\Delta G = -RT \ln K_d$$

(5)

where the symbols have their usual significance.

The thermodynamic behaviour of the sorption of Hg(II) onto BMAC from an aqueous solution indicates whether the sorption process follows physisorption or chemisorption [44]. The thermodynamic quantities ΔH, ΔS and ΔG for Hg(II) ion adsorption on activated carbon were calculated from the K_d values using Equations (3) and (4). Values of ΔH and ΔS were computed from the slope and intercept of linear variation of ln K_d with the reciprocal of temperature (Figure 9) and were found to be 19.65 kJ mol^{-1} and 113.90 kJ mol^{-1}, respectively. The positive sign of ΔH indicates the process to be endothermic, which is attributed to the increase in the diffusion rate of the adsorbate across the external boundary layer and internal pores of the adsorbent [45]. The low value of ΔH indicates the adsorption of Hg(II) ions on BMAC was dominated by the physisorption process [45]. The high positive value of ΔS indicates that a significant change in the internal structure of the activated carbon surface might have occurred at the solid-solution interface during the adsorption process owing to increased randomness [46]. The free energy of specific adsorption, ΔG, at various temperatures was calculated using Equation (4) and these are listed in Table 4. A negative ΔG value signifies the spontaneity of the adsorption process.

Table 4. Adsorption studies of Hg(II) ions on activated carbon as a function of temperature

T	1/T	K_d	ln	ΔG
(K)	(K-x10-3)	(mLg^{-1})	K_d	(kJmol^{-1})
298	3.38	290.2	5.67	-13.73
303	3.27	395.5	5.98	-14.97
308	3.22	457.4	6.125	-15.58
313	3.17	518.5	6.25	-16.16
318	3.1	584.1	6.37	-16.73
323	3.07	620.2	6.43	-17.15
328	2.9	925.2	6.83	-18.50
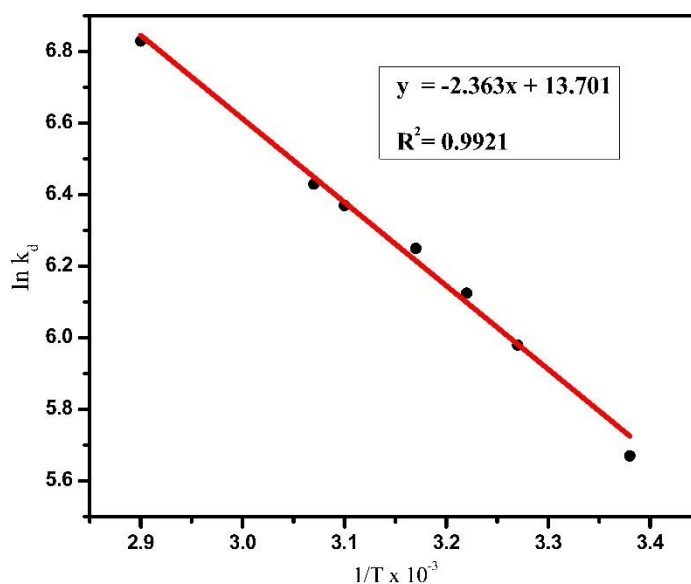
Figure 11. Plot of ln k_d vs 1/T. The slope and intercept give ΔH and ΔS respectively.

Best Fit Adsorption Isotherm Model Studies
Langmuir Adsorption Isotherm

This model describes a monolayer adsorption of adsorbate onto a homogeneous adsorbing surface characterized by uniform binding sites. It further postulates the absence of interactions between the adsorbed molecules while undergoing adsorption. The Langmuir isotherm is expressed in Equation (6):

$$q = \frac{q_{max}\, bC_{eq}}{1 + bC_{eq}} \tag{6}$$

The linear form of the Langmuir equation is given in Equation (7):

$$1/q = \frac{1}{q_{max}} + \frac{1}{\left(C_{eq} q_{max} b\right)} \tag{7}$$

where
C_{eq} = the equilibrium concentration of adsorbate (mg/L^{-1})
q = the amount of metal adsorbed per gram of adsorbent at equilibrium (mg/g).
q_{max} = maximum monolayer coverage capacity (mg/g)
b = Langmuir isotherm constant (L/mg).

The values of q and b were computed from the slope and intercept of the Langmuir plot of 1/Ce versus 1/qe (Figure 12) and the Langmuir parameters are given in Table 5.

The essential characteristics of the Langmuir isotherm can be expressed by a dimensionless constant called the separation factor R_L [47]:

$$R_L = \frac{1}{1 + bC_i} \tag{8}$$

where:
C_i = initial concentration
R_L = the constant related to the energy of adsorption (Langmuir Constant R_L value indicates the adsorption nature to be either unfavourable if $R_L > 1$, linear if $R_L = 1$, favourable if $0 < R_L < 1$)

From Figure 12 and Table 5, the R_L value for the fitted Langmuir isotherm was calculated to be 0.231. This value which lies between 0 and 1, indicating favourable adsorption.

Freundich Adsorption Isotherm

The Freundlich isotherm can be derived from the Langmuir isotherm by assuming that there exists a distribution of sites on the adsorbent that have different affinities for different adsorbates, with each site behaving according to the Langmuir isotherm. The model can be applied to multilayer adsorption with non-uniform distribution of heat and adsorption affinities over the heterogeneous surface. The Freundlich equation can be expressed as follows:

$$q_e = KC^{1/n} \tag{9}$$

where K is the measure of the capacity of the adsorbent (mass of adsorbate/mass of adsorbent) and n is a measure of how affinity for the adsorbate changes with adsorption density. $n > 1$ indicates the affinity decreases with increasing adsorption density. Evaluation of the coefficients of K and n
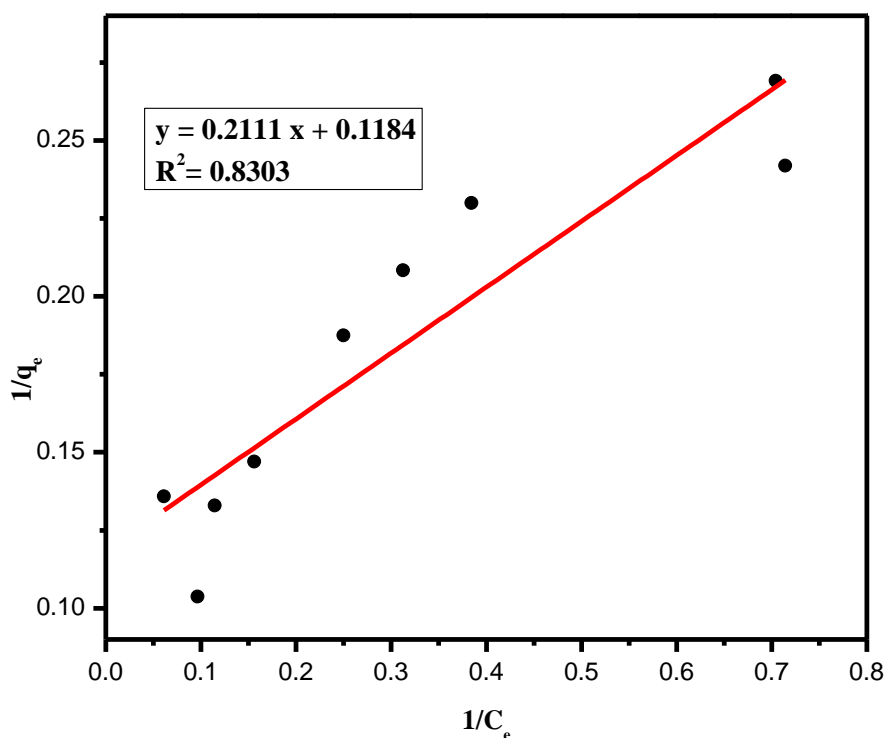
Figure 12. Langmuir adsorption isotherm plot for the adsorption of Hg(II) on BMAC.

can be accomplished using the linearized equation:

$$\log q_e = \log K + 1/n \log C_e \qquad (10)$$

The values for these parameters were calculated and plotted in Figure 13. The R^2 value obtained was 0.9921. The experimental data fits the isotherm adequately and the parameters are tabulated in Table 5.

The constant K is an approximate indicator of adsorption capacity, while 1/n is a function of the adsorption strength [47]. If n = 1, the partition between the two phases is independent of the concentration. If the value of 1/n is below one, it indicates normal adsorption. On the other hand, 1/n being greater than one indicates cooperative adsorption. From the plot in Figure 13, the 1/n value is calculated to be 0.353 and the n value corresponds to 2.83, indicating a normal adsorption process.

Temkin Adsorption Isotherm

The Temkin isotherm contains a factor that explicitly takes into account adsorbent–adsorbate interactions. By ignoring the extremely low and high concentrations, it further suggests that because of the interaction, the heat of adsorption of all the molecules in the layer would decrease linearly. The Temkin isotherm can be expressed using the Equation (11)

$$q_e = B \ln (AC_e) \qquad (11)$$

where B = RT/b, b is the Temkin constant and A is the equilibrium binding constant.

The linear form of the Temkin equation can be expressed in Equation (12):

$$q_e = B \ln A + B \ln C_e \qquad (12)$$
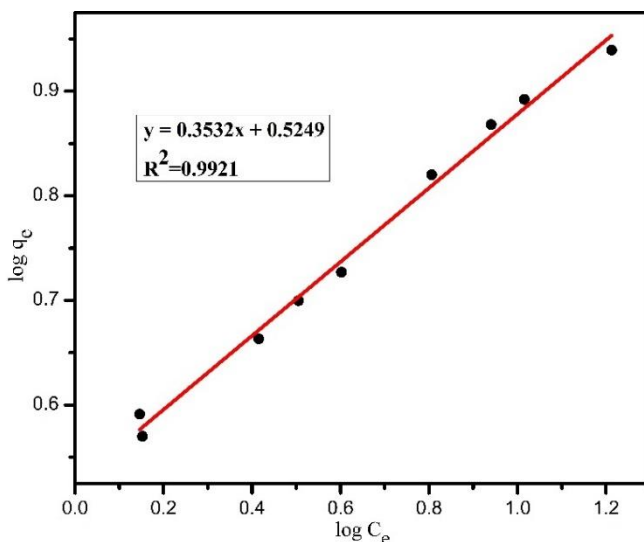
Figure 13. Freundlich adsorption isotherm plot for the adsorption of Hg(II) on BMAC.
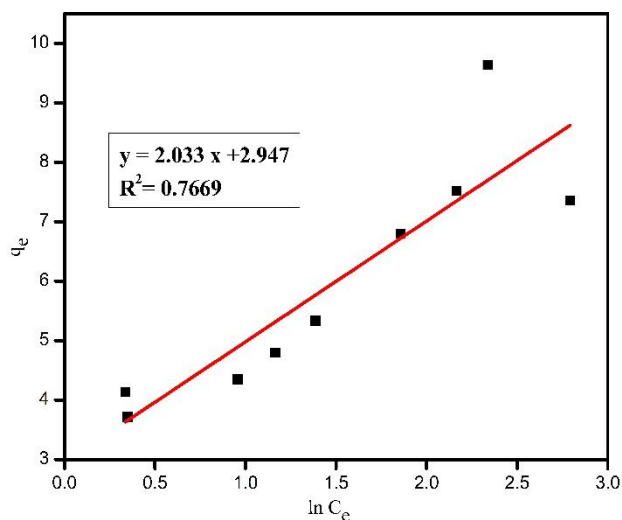
Figure 14. Temkin adsorption isotherm plot for the adsorption of Hg(II) on BMAC.

Table 5. Langmuir, Freundlich and Temkin parameter values for the adsorption of Hg(II) on BMAC.

Isotherm	Parameters	Value
Langmuir	q_{max} (mg/g)	4.12
	b (L/mg)	0.118
	R_L	0.231
	R^2	0.830
Freundlich	1/n	0.353
	K (mg/g)	3.492
	R^2	0.992
Temkin	A (L/g)	4.26
	B (J/mol)	2.033
	R^2	0.766

A plot of q_e against ln C_e (Fig. 14) gives the value of A and B. All the Temkin parameters are tabulated in Table 5.

From the Temkin plot shown in Figure 14, the following values were estimated: A = 4.26 L/g, B= 2.034 J/mol which indicates a physical adsorption process, with R^2=0.7669.

Calculation of the Order of the Adsorption Reaction

In this study, kinetic models were studied with different models to describe the kinetics of adsorption, including Zero order, First order, Second order, Third order, Pseudo First order and Pseudo Second order [48].

Zero Order

The differential equation which describes zero order is (FOGLER, 2006):

$$\frac{dc}{dt} = -K \quad (13)$$

Integrating with C = C_i at t = 0, yields

$$C_t = C_i - kt \quad (14)$$

where:
k is the rate constant of zero order adsorption (mg·L⁻¹·min⁻¹).
C_i and C_t are the liquid-phase concentrations of metal ions at the start and at time t, respectively (mg/L).
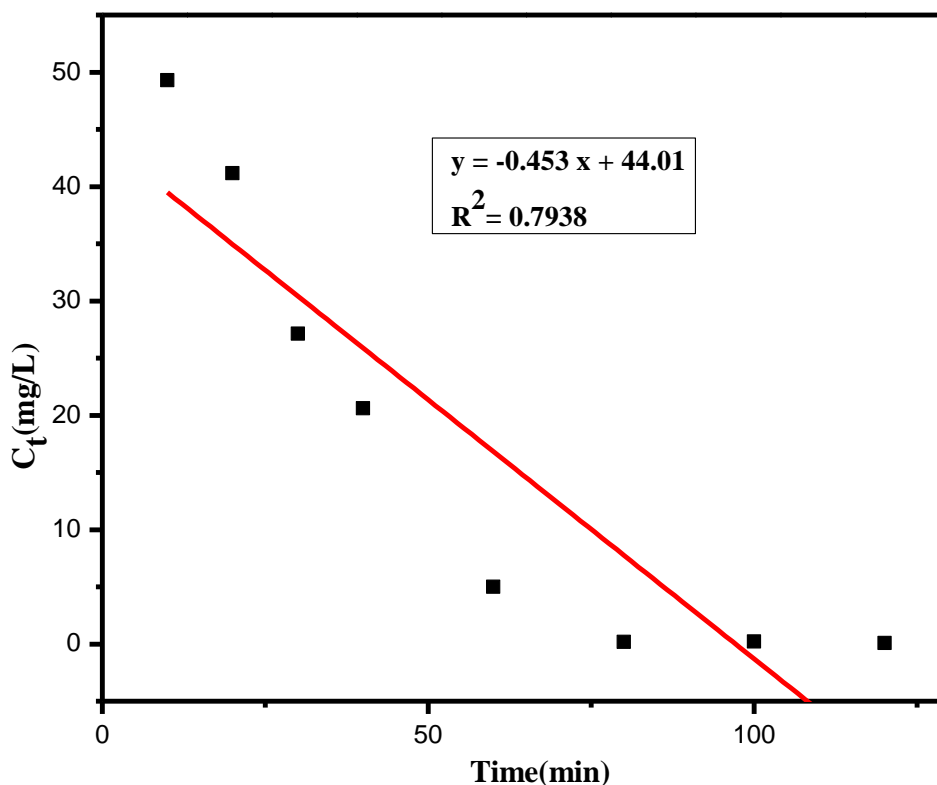
Figure 15. Zero order kinetics of Hg(II) ion adsorption on BMAC
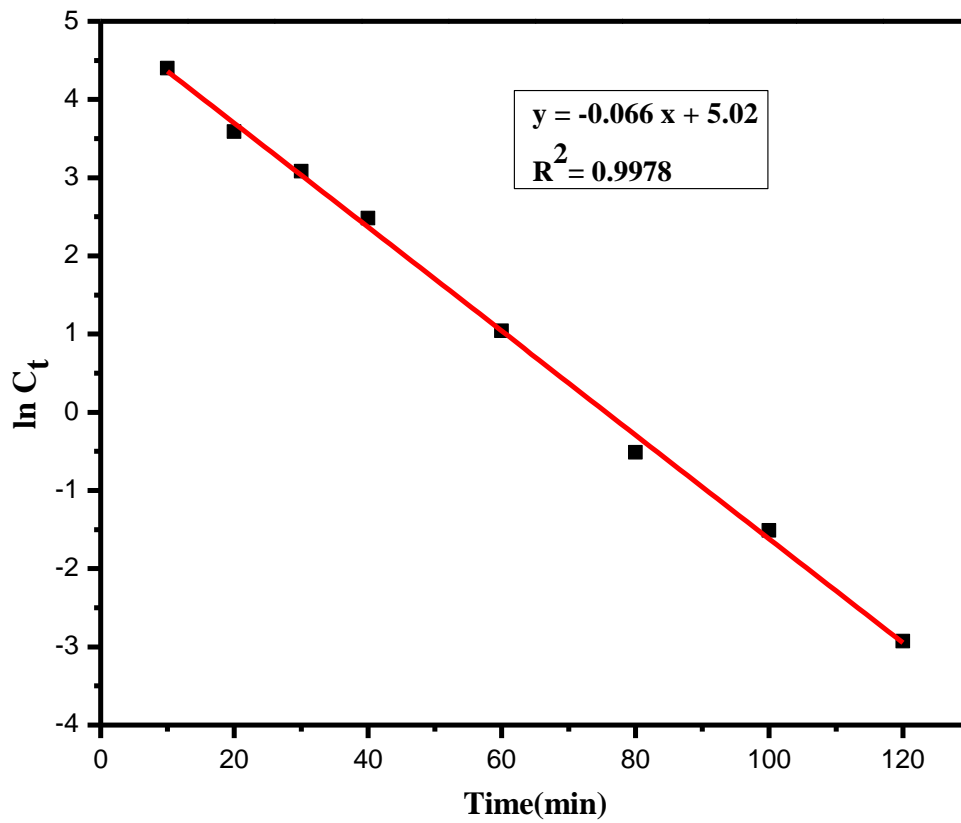
Figure 16. First order kinetics of Hg(II) ion adsorption on BMAC
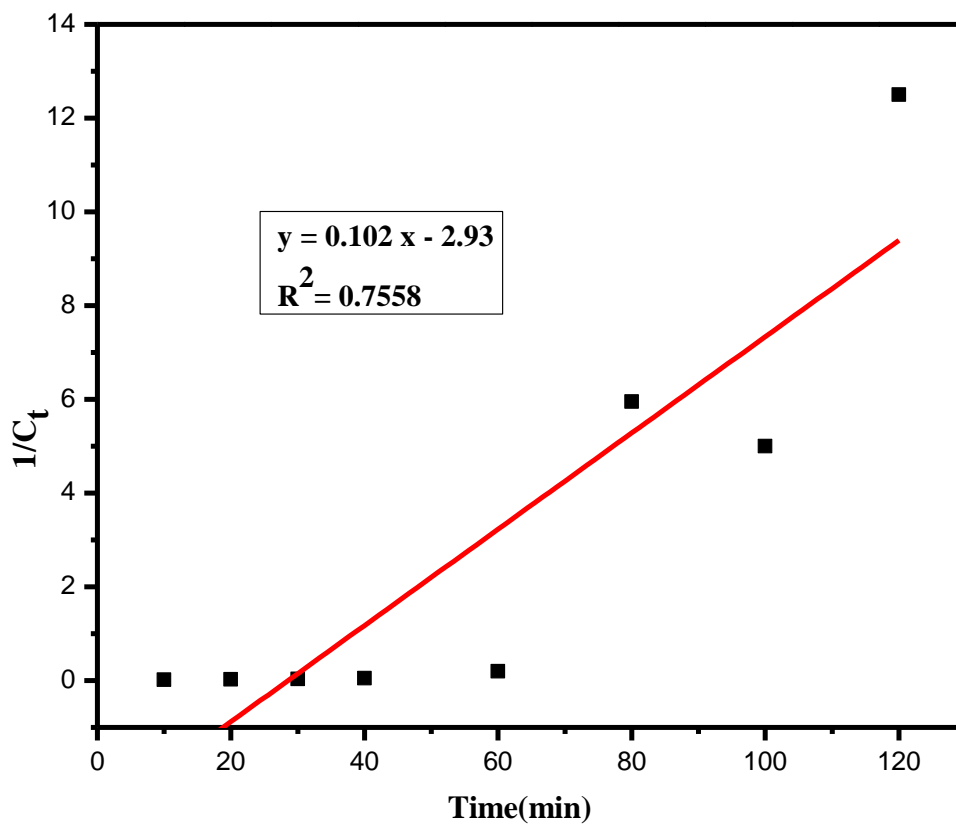
Figure 17. Second order kinetics of Hg(II) ion adsorption on BMAC

First Order

The differential equation which describes first order is (FOGLER, 2006):

$$\frac{-dC}{dt} = k_1 C \tag{15}$$

With the limit C= C_i at $t = 0$ gives

$$\ln C_t = \ln C_i - K_1 t \tag{16}$$

where K_1 is the rate constant of first order adsorption (min^{-1}).

Second Order

The differential equation which describes second order is (FOGLER, 2006; Ho et al., 2000):

$$\frac{-dc}{dt} = k_2 C^2 \tag{17}$$

With the limit C=C_i initially yields

$$\frac{1}{C_t} = \frac{1}{C_i} + K_2 t \tag{18}$$

Where

K_2 is the rate constant for second order adsorption (L·mg^{-1}·min^{-1}).

Third Order

The third order equation is given by the following (Ho et al., 2000):

$$\frac{1}{C_t^2} - \frac{1}{C_i^2} = k_3 t \tag{19}$$

where K_3 is the rate constant for third order adsorption (mg^2/L^{2}min^{-1}).

Pseudo First Order (Lagergren's Equation)

Lagergren's pseudo first order rate equation is the earliest known one describing the adsorption rate based on the adsorption capacity for liquid–solid phase adsorption systems. In order to distinguish kinetics equations based on concentrations of solution from adsorption capacities of solids, Lagergren's first order rate equation has been called pseudo first order. It is summarized as follows (Radniaet al., 2011; Ho & McKay, 1998):

$$\frac{dQ_t}{dt} = k_{1p} (Q_e - Q_t) \tag{20}$$

Where: k_{1p} is the rate constant of the pseudo first order adsorption (1/min).

On integrating the above equation, the linear form can be expressed as

$$\log (Q_e - Q_t) = \log Q_e - \frac{k_{1p}}{2.303} t \tag{21}$$
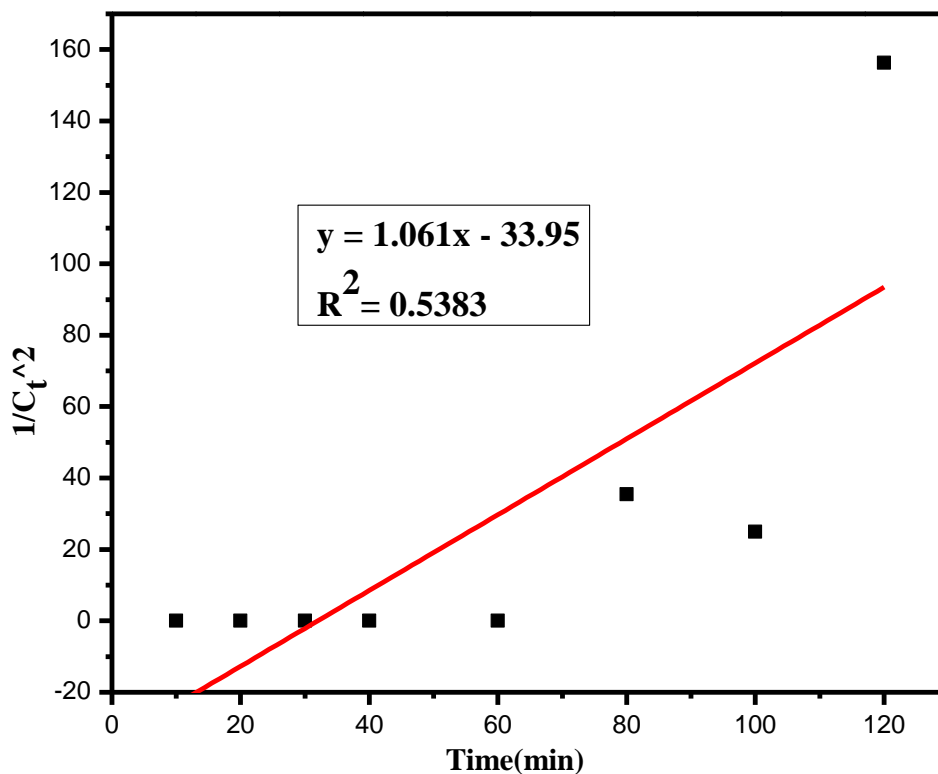
Figure 18. Third order kinetics of Hg(II) ion adsorption on BMAC
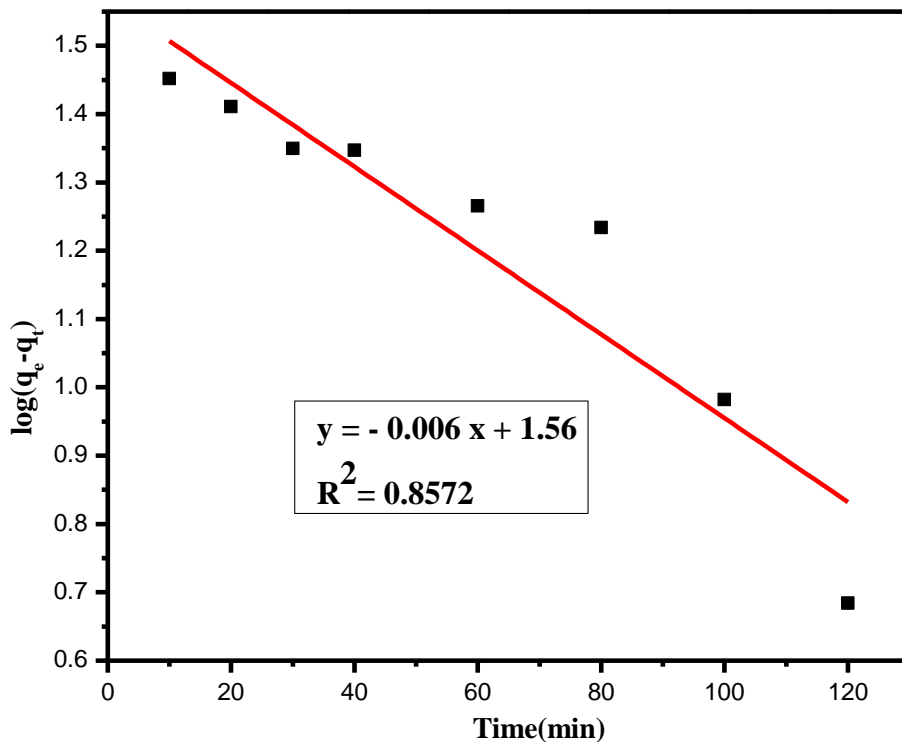
Figure 19. Pseudo first order kinetics of Hg(II) ion adsorption on BMAC

Pseudo Second Order (Lagergren's Equation)

The pseudo second order expression can be derived from Equation 22

$$\frac{dQ_t}{dt} = K_{2P}(Q_e - Q_t)^2 \tag{22}$$

where K_{2P} is the rate constant for adsorption (g.g^{-1}min^{-1}).

On integrating the above equation, the linear form can be expressed as follows

$$\frac{t}{Q_t} = \frac{1}{k_{2p}Q_e{}^2} + \frac{1}{Q_e}t \tag{23}$$
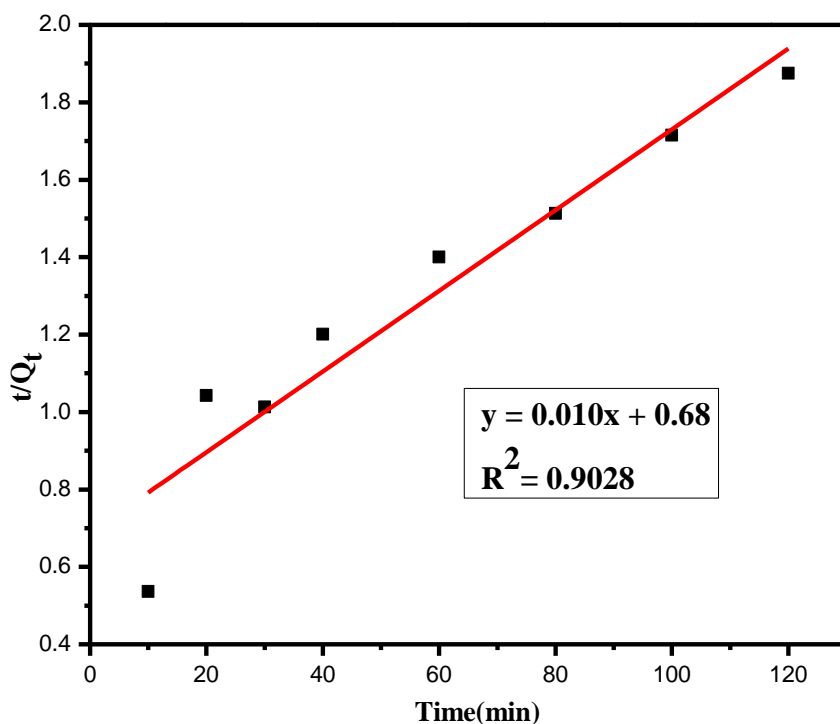
Figure 20. Pseudo second order kinetics of Hg(II) ion adsorption on BMAC

Table 6. The kinetic models of adsorption of Hg(II) ion on the BMAC.

Order of the reaction	K	R^2
Zero Order	0.453	0.7938
First Order	0.066	0.9978
Second Order	0.102	0.7558
Third Order	1.061	0.5383
Pseudo First Order	0.006	0.8572
Pseudo Second Order	0.010	0.9028

The study of adsorption kinetics describes the metal uptake rate, and evidently this rate controls the residence time of the adsorbate at the solid–solution interface, including the diffusion process. For the adsorption of Hg(II) ion on BMAC, the parameters for the zero order, first order, second order, pseudo first order and pseudo second order adsorption kinetic models are listed and compared in Table 6. As we can see from Figures 15-20, among all the kinetic models, first order kinetics was best suited to the experimental data and helps in understanding the adsorption process with a correlation value of 0.9978. This is very close to 1, which indicates that the Hg(II) ion adsorption process fits the first order kinetic model very well.

CONCLUSION

This work demonstrates the efficacy of BMAC, derived from low cost and highly abundant *Calotropis procera* stems, as a potent bioadsorbent after simultaneous impregnation and activation with (1:9, 2:8, 3:7) H_2SO_4 and H_3PO_4 under laboratory-feasible conditions. Proximate analysis of BMAC revealed its low ash content (28.50 %), low apparent density (0.35 g/ml) and high ion exchange capability (1.02 meqv/g), all properties which are desirable for a high-quality carbon. The characterisation results provide evidence of the successful impregnation and functionalisation of SO_4^{3-} and PO_4^{3-} on BMAC. SEM and BET results demonstrated that the irregular cave-type openings corresponding to a large pore size and high surface area of 524 m^2/g were achieved by pulverizing the activated carbon to nanosize by ball milling. The optimum set of parameters were determined to be 120 min contact time, adsorbent dose of 4 g, Hg(II) ion concentration of 20 mg/L, and a pH 4 solution, maintained at 60 °C. The adsorption of Hg(II) ion on BMAC was found to be 99%. The experimental results complied with the Freundlich Isotherm model and First order kinetics. The positive ΔH and negative ΔG values obtained indicate the adsorption process was endothermic and spontaneous.

ACKNOWLEDGMENT

REFERENCES

1. Ali, H., Ezzat, K., Ikram, I. (2019) Environmental Chemistry and Ecotoxicology of Hazardous Heavy Metals: Environmental Persistence, Toxicity, and Bioaccumulation. *J. Chem.,* 1–14. https://doi.org/ 10.1155/2019/6730305

2. Jessica, B., Emmanuel, S., Renald, B. (2020) Heavy metal pollution in the environment and their toxicological effects on humans. *Heliyon*, **6**, 1–26. https://doi.org/10.1016/j.heliyon.2020.e04691

3. Oscar, D., Salcedo, C., DianaVargas, P., Giraldo, L. and Juan Carlos, M. P. (2021) Study of Mercury [Hg(II)] Adsorption from Aqueous Solution on Functionalized Activated Carbon. *Acs Omega*, **6**, 11849–11856. https://doi.org/10.1021/acsomega.0c 06084

4. Rameshraja, D., Vimal Chandra, S., Jai Prakash, K., Indra, D. M. (2017) Competitive adsorption isotherm modelling of heterocyclic nitrogenous compounds, pyridine and quinoline, onto granular activated carbon and bagasse fly ash. *Chem. Pap.*, **72**, 617–628. 10.1007/s11696-017-0321-6

5. Grégorio, C., Eric, L. (2019) Advantages and disadvantages of techniques used for wastewater treatment. Environ. *Chem. Lett.*, **17**, 145–155. 10. 1007/s10311-018-0785-9

6. Dr. Sumita, M., Dr. Jayant, B. (2007) Batch Studies on Phenol Removal using Leaf Activated Carbon. *Malays. J. Chem.*, **9**, 051–059.

7. Rajan, A., Sanju, S., Dr. Babu, V. (2016) Solvent Extraction and Adsorption technique for the treatment of Pesticide effluent. *CiVEJ*, **3**, 155–165.

8. Azizul, H. L., Rohana, A., Mohd. Mansor, H., Nur Farah Waheed, T., Norazzizi, N. (2020) Adsorption Kinetics for Carbon dioxide Capture using Bismuth(III) Oxide Impregnated on Activated Carbon. *Malays. J. Chem.*, **22**, 33–46.

9. Maharana, M., Manna, M., Sardar, M., Sen, S. (2021) Heavy metal removal by low-cost adsorbents. InGreen Adsorbents to Remove Metals, Dyes and Boron from Polluted Water.

Springer, Cham., 245–272.

10. Yafei, G., Chang, T., Jian, S., Weiling, L., Jubing, Z., Chuanwen, Z. (2020) Porous activated carbons derived from waste sugarcane bagasse for CO2 adsorption. *Chem. Eng. J.*, **381**, 1–9. https://doi.org/ 10.1016/j.cej.2019.122736

11. Yan, H., Andrew, P., John, S. (2000) Acid-Treated Soy Hull Carbon Structure and Adsorption Performance. *JAOCS*, **77**, 785–790. 10.1007/s11 746-000-0125-2

12. Jiang, Y. (2017) Preparation of activated carbon from walnut shell and its application in industrial wastewater. *InAIP Conference Proceedings, IP Publishing LLC*, 1839(1), 020063.

13. Sartova, K., Omurzak, E., Kambarova, G., Isaak, D., Bakyt, B., Zhypargul, A. (2018) Activated Carbon obtained from the Cotton Processing Wastes. *DIAMAT*, **7255**, 1–23. https://doi.org/10. 1016/j.diamond.2018.11.011

14. William, B., Jennifer, M., Samuel, N. (2016) Conversion of Corn Cobs Waste into Activated Carbons for Adsorption of Heavy Metals from Minerals Processing Wastewater. *IJEPP*, **4**, 98–103. 10.11648/j.ijepp.20160404.11

15. Suhas, Gupta, V. K., Carrott, P. J. M., Randhir, S., Monika, C., Sarita, K. (2016) Cellulose: A review as natural, modified and activated carbon adsorbent. *Bioresour. Technol.*, **216**, 1066–1076. http://dx.doi.org/10.1016/j.biortech.2016.05.106

16. Budinova, T., Ekinci, E., Yardim, F., Grimm, A., Björnbom, E., Minkova, V., Goranova, M. (2006) Characterization and application of activated carbon produced by H_3PO_4 and Water vapor activation. *Fuel Process. Technol.*, **87**, 899–905. 10.1016/j. fuproc.2006.06.005

17. Moulefera, Francisco, J., García, M., Abdelghani, B., Rosas, J. M., Rodríguez, J. M., Cordero, T. (2020) Effect of Co-solution of Carbon Precursor and Activating Agent on the Textural Properties of Highly Porous Activated Carbon Obtained by Chemical Activation of Lignin with H_3PO_4. Front. *Mater.*, **7**, 153–167. https://doi.org/10. 3389/fmats. 2020.00153

18. Prakash, P., Hamish, R. M., Sabah, M., Shifa, Z., Tareq Al, A., Gordon, M. (2021) Char Products from Bamboo Waste Pyrolysis and Acid Activation Front. *Mater.*, **7**, 624791–624806. 10.3389/fmats. 2020.624791

19. Kolur, N. A., Seyedmehdi, S., Kaghazchi, T. (2019) Investigation of sulfuric acid-treated activated carbon properties. *Turk J Chem.*, **43**, 663–675.

20. Ademiluyi, F. T., David, E. O. (2012) Effect of Chemical Activation on the Adsorption of Heavy Metals Using Activated Carbons from Waste Materials. *ISRN Chem. Eng.*, 674209–674214. 10.5402/2012/674209

21. Zakaria, R., Nur Azimah, J., Zailani-Abu, M. B. (2021) Effect of impregnation ratio and activation temperature on the yield and adsorption performance of mangrove based activated carbon for methylene blue removal. *Mater. Today*, **10**, 100183–100194. https://doi. org/10.1016/j.rinma. 2021.100183

22. Pawel, G., Katarzyna, Z., Wagner-Doebler, B., Stanislaw, L. (2008) Bioreduction of ionic mercury from wastewater in a fixed-bed bioreactor with activated carbon. *Chem. Pap.*, **62**, 232–238. 10. 2478/s11696-008-0017-z

23. Erdman, M. D., Erdman, B. A. (1981) *Calotropis procera* as a Source of Plant Hydrocarbons. *Econ. Bot.*, **35**, 467–472. http://www.jstor.org/stable/425 4326

24. Kaur, A., Batish, D. R., Kaur, S., Chauhan, B. S. (2021) An Overview of the Characteristics and Potential of *Calotropis procera* From Botanical, Ecological, and Economic Perspectives. *Front. Plant Sci.*, **12**, 690806. doi: 10.3389/fpls.2021. 690806

25. Zhiyuan Liu, Yong Sun, Xinrui Xu, Jingbo Qu, Bin Qu (2020) Adsorption of Hg(II) in an Aqueous Solution by Activated Carbon Prepared from Rice Husk Using KOH Activation. *ACS Omega*, **5**, 29231−29242. https://dx.doi.org/10. 1021/acso mega.0c03992

26. Yakout, S. M., El-Deen, G. S. (2016) Characterization of activated carbon prepared by phosphoric acid activation of olive stones. *Arab. J. Chem.*, **9**, S1155–S1162. http://dx.doi.org/10. 1016/j.arabjc.2011.12.002

27. Himanshu, P. (2021) Review on solvent desorption study from exhausted adsorbent. *J. Saudi Chem. Soc.*, **25**, 101302–101311. https:// doi.org/10.1016/j. jscs.2021.101302

28. Sumrit, M., Nuchjira, D. (2021) Activated carbon preparation from eucalyptus wood chips using continuous carbonization–steam activation process in a batch intermittent rotary kiln. *Sci. Rep.*, **11**, 13948–13957. https://doi.org/10.1038/s41598-021–93249-x

29. Rodríguez-Vidal, F. J., Azabache, B. O., Ángela González, M., Fernández, A. B. (2022) Comprehensive characterization of industrial wastewaters using EEM fluorescence, FT-IR and 1H NMR techniques. *Sci. Total Environ.*, **805**,

150417–150429. https://doi.org/10.1016/j.scito
tenv. 2021.150417

30. Roonasi, P., Adsorption and surface reaction
    properties of synthesized magnetite nano-
    particles (Doctoral dissertation, Luleå tekniska
    universitet).

31. Hadjiivanov, K. I., Dimitar Panayotov, A.,
    Mihail, Y., Elena Ivanova, M. Z., Kristina, K. C.,
    Stanislava, M. A., Nikola, L. D. (2021) Power of
    Infrared and Raman Spectroscopies to
    Characterize Metal-Organic Frameworks and
    Investigate Their Interaction with Guest
    Molecules. *Chem. Rev.*, **121**, 1286−1424. 10. 1021/
    acs.chemrev.0c00487

32. Yanping, G., David, A. (2006) Rockstraw
    Activated carbons prepared from rice hull by
    one-step phosphoric acid activation. *Micro-
    porous Mesoporous Mater.*, **100**, 12–19. 10.1016
    /j.micromeso.2006.10.006

33. Yorgun, S., Derya, Y. (2015) Preparation and
    characterization of activated carbons from
    Paulownia wood by chemical activation with
    H3PO4. *J Taiwan Inst Chem Eng.*, **53**, 122–131.
    https://doi.org/10.1016/j.jtice.2015.02.032

34. Oleg, P., Tudor, L., Dominika, B., Igor, P.,
    Tatiana, M., Maria, R. (2019) Microbiological
    Properties of Microwave-Activated Carbons
    Impregnated with Enoxil and Nanoparticles of
    Ag and Se. C. **5**, 31–44. 10.3390/c5020031

35. Teruaki, Y., Hisashi, M. (2014) Reaction
    behavior of wood in an ionic liquid, 1-
    ethylpyridinium bromide. *J Wood Sci.*, **60**, 339–
    345. 10.1007/s10086-014-1409-z.

36. Athiwat, S., Atong, D., Chiravoot, P. (2012)
    Comparison on Pore Development of Activated
    Carbon Produced from Scrap Tire by Hydro-
    chloric Acid and Sulfuric Acid. *Adv Mat Res.*,
    626, 706–710. https://doi.org/10.4028/www.
    scientific.net/AMR.626.706.

37. Mengdan Xi, Chen, Z., Yao Li, Chuanhua Li,
    Nasir M. Ahmad, Cheemad, A., Shenmin Zhu
    (2019) Removal of Hg(II) in aqueous solutions
    through physical and chemical adsorption
    principles. *RSC Adv.*, **9**, 20941–20953. 10.
    1039/c9ra01924c

38. Kuang, Y., Zhang Xi, Shaoqi, Z. (2020)
    Adsorption of Methylene Blue in Water onto
    Activated Carbon by Surfactant Modification.
    Water, **12**, 587. doi:10. 3390/w12020587

39. Vinod, K. G., Deepak, P., Shikha, S. (2013)
    Adsorptive remediation of Cu(II) and Ni(II) by
    microwave assisted H3PO4 activated carbon.
    Arab. J. Chem., **10**, S2836–S2844. http://dx.doi.

org/10.1016/j.arabjc.2013.11.06

40. Chao, L., Jinhui, P., Libo, Z., Shixing, W.,
    Shaohua, J., Chenhui, L. (2018) Mercury
    adsorption from aqueous solution by regenerated
    activated carbon produced from depleted
    mercury-containing catalyst by microwave-
    assisted decontamination. *J. Clean. Prod.*, **196**,
    109–121. https://doi.org/10.1016/j. jclepro.2018.
    06.027 0959-6526

41. Al-Ghout, M. A., Dana, D., Dieyeh, M. A.,
    Majeda, K. (2019) Adsorptive removal of
    mercury from water by adsorbents derived from
    date pits. *Scientific Reports*, **9**, 15327–15340.
    https://doi.org/ 10.1038/s41598-019-51594-y

42. Lalhmunsiama, Seung Mok Lee, Suk Soon, C.
    and Diwakar, T. (2017) Simultaneous Removal
    of Hg(II) and Phenol Using Functionalized
    Activated Carbon Derived from Areca Nut
    Waste. *Metals*, **7**, 248. 10.3390/met7070248

43. Jyotsna, G., Kadirvelu, K., Rajagopal, C. (2004)
    Mercury (II) removal from water by coconut
    shell based activated carbon: Batch and column
    studies. *Environmental Technology*, **25(2)**, 141–
    153. 10.10 80/09593330409355447.

44. Nasser Sahmoune, M. (2018) Evaluation of
    thermo-dynamic parameters for adsorption of
    heavy metals by green adsorbents. *Environ.
    Chem. Lett.* https://doi.org/10.1007/s10311-018-
    00819-z.

45. Igberase, E., Osifo, P., Ofomaja, A. (2017)
    The Adsorption of Pb, Zn, Cu, Ni, and Cd by
    Modified Ligand in a Single Component
    Aqueous Solution: Equilibrium, Kinetic, Thermo-
    dynamic, and Desorption Studies. *International
    Journal of Analytical Chemistry*, **6150209**. https:
    //doi.org/10.1155/2017/6150209

46. Foad, R., Majid, P. (2014) Kinetic and thermo-
    dynamic studies of Hg(II) adsorption onto
    MCM-41 modified by ZnCl$_2$. *Appl. Surf. Sci.*,
    301, 568–575. https://doi.org/10.1016/j.apsusc.
    2014.02.136

47. Sivakumar, S., Muthirulan, P., Meenakshi Sundaram,
    M. (2019) Adsorption kinetic and isotherm
    studies of Azure A on various activated carbons
    derived from agricultural wastes. *Arab. J. Chem.*,
    12, 1507–1514.

48. Chunfang, T., Shu, Y., Zhang, R., Xin Li, Song,
    J., Bing Li, Zhanga, Y., Danling, O. (2017)
    Comparison of the removal and adsorption
    mechanisms of cadmium and lead from aqueous
    solution by activated carbons prepared from
    Typha angustifolia and Salix matsudana. *RSC
    Adv.*, **7**, 16092–16103. 10.1039/c6ra28035h.